Geophysical Research Letters

RESEARCH LETTER
10.1029/2024GL113807

Interannual Variability of Tropical Cyclone Landfalls in the Eastern North Pacific: Environmental Drivers and Implications

Jose A. Ocegueda Sanchez[1], **Daniel R. Chavas**[1], **and Jhordanne J. Jones**[2]

[1]Department of Earth, Atmospheric, and Planetary Sciences, Purdue University, West Lafayette, IN, USA, [2]Department of Physics, University of the West Indies, Kingston, Jamaica

Key Points:

- The Eastern North Pacific seasonal cycle has a bimodal distribution of tropical cyclone landfalls due to its orography
- During high landfall years, tropical cyclones make landfall in vulnerable Southern Mexico due to a stronger reversal of the easterlies
- Steering wind anomalies are the main driver for landfall interannual variability in the East Pacific

Supporting Information:

Supporting Information may be found in the online version of this article.

Correspondence to:

J. A. Ocegueda Sanchez,
jocegue@purdue.edu

Citation:

Ocegueda Sanchez, J. A., Chavas, D. R., & Jones, J. J. (2025). Interannual variability of tropical cyclone landfalls in the Eastern North Pacific: Environmental drivers and implications. *Geophysical Research Letters*, *52*, e2024GL113807. https://doi.org/10.1029/2024GL113807

Received 19 NOV 2024
Accepted 14 APR 2025

Author Contributions:

Conceptualization: Jose A. Ocegueda Sanchez, Daniel R. Chavas
Data curation: Jose A. Ocegueda Sanchez
Formal analysis: Jose A. Ocegueda Sanchez, Daniel R. Chavas
Funding acquisition: Daniel R. Chavas
Investigation: Jose A. Ocegueda Sanchez
Methodology: Jose A. Ocegueda Sanchez, Daniel R. Chavas, Jhordanne J. Jones
Project administration: Daniel R. Chavas
Resources: Daniel R. Chavas
Software: Jose A. Ocegueda Sanchez, Jhordanne J. Jones
Supervision: Daniel R. Chavas
Validation: Jose A. Ocegueda Sanchez, Daniel R. Chavas, Jhordanne J. Jones
Visualization: Jose A. Ocegueda Sanchez, Jhordanne J. Jones

Abstract Despite its high tropical cyclone (TC) density, the Eastern North Pacific (ENP) basin has received relatively little research attention on landfall variability. This study investigates the climatological seasonal cycle and interannual variability of TC landfalls in the ENP. We find that the basin is characterized by a bimodal distribution of landfalls, with peaks in June and September–October. Using a composite analysis of high and low landfall years, we show that this distribution is primarily driven by landfall probability rather than genesis. The absence of landfalls during July is due to enhanced easterlies from the Caribbean Low-Level Jet entering the ENP through gaps in the Americas Cordillera. High landfall years feature enhanced easterly wind reversals from a northward-shifted Intertropical Convergence Zone. These additional steering winds drive hurricanes ashore in the vulnerable region of southwest Mexico. This study provides valuable insights for improving TC landfall forecasts and preparedness in the region.

Plain Language Summary Two to three storms strike the tropical Pacific coast of the Americas each year on average, but the reasons behind the interannual variability of landfalling events remain unclear. We found that landfalls occur in two main periods: June and then again in September and October. This two-peak pattern is due to changes in wind direction that either steer storms toward the coast or push them away. In July, strong easterly winds from the Caribbean prevent storms from reaching land, resulting in the double peak distribution of landfalls. During years with more landfalls, the tropical rain belt in the basin is farther north than usual, driving more eastward flow that guides storms into the vulnerable region of southwest Mexico. By identifying the atmospheric patterns during high landfall years, our study can help improve storm forecasts in the region and aid communities in better preparing for extreme weather events.

1. Introduction

Despite being an eastern basin surrounded by cold waters, the Eastern North Pacific (ENP, east of 140°W) is the basin with the highest density (number of storms per unit area) of tropical cyclones (TCs) in the world (Sobel et al., 2021; Zhao et al., 2020). Although it is a highly active basin, the ENP receives relatively little research attention compared to other basins, particularly regarding landfall. Most studies have focused on TC activity under different climate modes, with some identifying conditions that might be favorable for genesis location (Camargo et al., 2008; Collins & Mason, 2000, 2003). However, no study has purely focused on understanding landfall variability within the basin, possibly because most storms move northwest away from the coastline.

The lack of research in this area is significant because landfalling TCs can have severe socioeconomic impacts, both at landfall and for several months afterward, affecting services such as food supply and transportation (Dominguez et al., 2021; Juarez-Torres & Puigvert, 2021). Furthermore, landfalling TCs and their remnants significantly contribute to precipitation: up to 30% in northwestern Mexico, 20% in southern California, 10% in southwestern Mexico, and 5% in New Mexico (Corbosiero et al., 2009; Dominguez & Magaña, 2018).

In the ENP, the TC season is defined to start in mid-May and end in November (Romero-Vadillo et al., 2007). Previous research (Boucharel et al., 2016; Fu et al., 2017; Kim et al., 2011) has shown that during El Niño (the opposite for La Niña), particularly East Pacific Warming, the number of named storms increases in the western part of the basin while slightly decreasing in the eastern part of the basin.

Tropical cyclones move following the steering wind, a vertically integrated measure of the surrounding flow, with a slight deviation to the northwest due to the beta effect (meridional gradient of the Coriolis force) (Chan, 2005).

Writing – original draft: Jose A. Ocegueda Sanchez
Writing – review & editing: Jose A. Ocegueda Sanchez, Daniel R. Chavas, Jhordanne J. Jones

On Earth, constant trade wind easterlies facilitate landfall along eastern coasts; however, the ENP differs with land to the east of TC formation, where a weakening of the easterly flow is needed to steer a storm onto land. Note that, while storms from the ENP have threatened or impacted Hawaii (e.g., Hurricane Douglas 2020), our study focuses on the Pacific coastline of the Americas.

Besides the trade winds, another recurrent feature of the tropical large-scale circulation is the presence of monsoons. Previous studies (Camargo et al., 2007; Carr & Elsberry, 1995; Ito et al., 2020) in the Western North Pacific and idealized simulations have shown that, depending on the intensity and relative location of monsoon troughs and gyres, TCs can experience a sudden northward movement when they are positioned east of the center of the monsoon system. The ENP is also characterized by two monsoon systems: the well-known subtropical North American monsoon that develops in the Gulf of Baja California and a tropical monsoon (although Geen et al. (2020) suggested calling this system an ITCZ extension), which is closer to the equator and starts to develop near Central America (Zhisheng et al., 2015).

Furthermore, gaps in the American Cordillera (Tehuantepec, Papagayo, and Panama) allow strong interbasin influences due to Central America Gap Winds (CAGW), which are intense low-level flows channeled through narrow mountain passes. CAGW are strongest during winter and transport moisture to the ENP modulating convection and precipitation (Fu et al., 2017; Xie et al., 2005; Yang et al., 2017). However, the CAGW also reach a secondary peak in midsummer, linked to the Caribbean Low-Level Jet (CLLJ) crossing at Papagayo and contributing to the midsummer drought, when rainfall briefly diminishes across Central America around July–August (Romero-Vadillo et al., 2007). Figure 4b illustrates the interaction between ITCZ monsoonal winds, the CLLJ, and the CAGW.

Some studies (Camargo et al., 2008; Fu et al., 2017; W. Li et al., 2015) have pointed out conditions (such as different MJO phases, the Interdecadal Pacific Oscillation, and ENSO) that might increase the likelihood of landfall based on genesis location. Additionally, it has been suggested (Corbosiero et al., 2009; W. Li et al., 2015) that the steering flow plays a more important role (in the ENP) in determining landfall probability for a given storm than its genesis location.

However, what governs the climatological seasonal cycle of TC landfall and its interannual variability in the ENP has not been studied. Understanding this better would improve forecasting and help society better prepare for the impacts of these storms, particularly in vulnerable regions across the Pacific coast. This study aims to fill this research gap by analyzing how variations in genesis and steering flow contribute to variations in landfall during years of high and low landfall activity in the ENP. Our main research questions are the following:

1. What is the climatological seasonal cycle of TC landfalls in the ENP? To what extent do genesis anomalies versus steering wind anomalies control this cycle?
2. Where is the preferred location of landfall in the basin? Does this location depend on the yearly landfall probability?
3. Do the monsoonal winds, as the main source of westerlies in the basin, significantly contribute to the interannual variability of landfall in the ENP?

To answer these questions, we perform a composite analysis of two groups of years based on their yearly number of landfalls and landfall probability, quantifying the contributions of genesis and steering winds to total landfall counts and comparing the mean environmental differences between them. The structure of this paper is as follows. First, in Section 2, we describe the data and methods used in this study, followed by the key findings in the results section. Finally, we discuss these results in the context of existing literature, and their implications for the communities along the Pacific coastline.

2. Methods

2.1. Data

For historical climate data, we use the monthly mean surface, pressure-level, and mean fluxes from the fifth-generation ECMWF reanalysis (ERA5) data on NCAR's Research Data Archive (RDA) from 1980 to 2024 (ECMWF, 2019). We choose ERA5 for its high spatial resolution, which is important for TC activity in the ENP, as demonstrated by previous studies (e.g., Fu et al., 2021). Moreover, compared to other reanalysis products,

ERA5 better captures precipitation in the ITCZ of the ENP (Huaman et al., 2022), which we use to locate the monsoon location in our composites.

For TC records (trajectory and intensity), we use the International Best Track Archive for Climate Stewardship (IBTrACS) data set version 04r01 for the East Pacific basin (Gahtan et al., 2024). The genesis location is defined in this study as the moment in which a storm reaches tropical storm intensity (1-min maximum sustained wind speed, $v_{max} \geq 17.5$ m/s), in the Eastern North Pacific (East of 140°W and West of Pacific America's coastline). With this definition of genesis we don't consider storms that form in the Atlantic and cross the continent to the Pacific. We used the landfall location given in the IBTrACS data set; for storms that make more than one landfall, we considered the landfall location as the landfall in which the storm was strongest before reaching the coastline, that is, we are only considering one landfall per storm.

2.2. Analysis

First, we start defining two subgroups of years between 1980 and 2024 based on their number of landfall events (N_{lf}) defined here as the product of the total number of storms (N_{gen}) and the landfall probability for each period (p_{lf}):

$$N_{lf} = p_{lf} N_{gen}, \tag{1}$$

high landfall years (hereafter HLY) are defined as the years that fall in the highest quartile of landfall count (which corresponds to $N_{lf} \geq 4$), while low landfall years (LLY) are those in the lowest quartile ($N_{lf} \leq 1$).

To assess the regions affected by TCs during both groups of years, we use an adjusted (to work with all countries in the ENP) version of the storm wind model developed by Anderson et al. (2021) that uses the parametric wind model derived by Willoughby et al. (2006) to estimate v_{max} at the centroid of each second-level administrative division. We choose to use this wind model since other models such as C15 (Chavas et al., 2015) require either the radius of maximum winds or the radius of gale force winds, and early data of IBTrACS only have the v_{max} and minimum pressure and these may not be independent measurements. The use of a parametric wind model is reasonable in the ENP since the storms in this basin are relatively small and have the smallest variance in size across basins (Chavas et al., 2016).

To analyze the differences in the number of landfalls between HLY and LLY, we perform a Reynolds decomposition on Equation 1 to quantify the contributions from genesis and landfall probabilities as follows:

$$N_{lf} = \overline{N_{gen}}\,\overline{p_{lf}} + \overline{N_{gen}} p'_{lf} + N'_{gen}\,\overline{p_{lf}} + N'_{gen} p'_{lf}, \tag{2}$$

Here, the bar quantities represent the climatological mean, and the prime quantities are the anomalies (deviations) from the climatology. Subsequently, we perform a box analysis to examine the contributions of each quantity within i different regular boxes of 5° × 5°, so the total number of landfalls between the two groups of years is given by

$$\Delta N_{lf} = \sum_i \begin{aligned} &\underbrace{\overline{N^i_{gen}}\left(p^{i\prime}_{lf,HLY} - p^{i\prime}_{lf,LLY}\right)}_{\text{Landfalls due to } p_{lf} \text{ anomalies}} + \\ &\underbrace{\overline{p^i_{lf}}\left(N^{i\prime}_{gen,HLY} - N^{i\prime}_{gen,LLY}\right)}_{\text{Landfalls due to } N_{gen} \text{ anomalies}} + \\ &\underbrace{N^{i\prime}_{gen,HLY}\, p^{i\prime}_{lf,HLY} - N^{i\prime}_{gen,LLY} p^{i\prime}_{lf,LLY}}_{\text{Residual}}. \end{aligned} \tag{3}$$

Simultaneously, we use ERA5 data to analyze the difference in steering winds, $\Delta \mathbf{V}_{steer} = \alpha \Delta \mathbf{V}_{850} + (1 - \alpha)\Delta \mathbf{V}_{250}$, where $\alpha = 0.8$, and $\mathbf{V}_{850}$ and $\mathbf{V}_{250}$ are the wind fields at 850 and 250 hPa, respectively. Note that we use a constant beta drift contribution following Emanuel et al. (2006), so the differences vanish. We also performed the same analysis using the optimal pressure weights for the ENP found in

DeMaria et al. (2022) and found that it produced qualitatively similar results. Therefore, for simplicity and ease of interpretation, we present the results using the simpler method outlined above.

To show the tropical monsoon region in the ENP, we calculated the Dynamical Seasonality Index (DNS), a quantity that captures the seasonal reversal of the prevailing winds, a common characteristic of monsoonal regions in the world (Zhisheng et al., 2015), that is defined in J. Li and Zeng (2003) as follows:

$$DNS = \frac{\|\overline{\boldsymbol{V}}_1 - \overline{\boldsymbol{V}}_7\|}{\|\overline{\boldsymbol{V}}\|} - 2, \tag{4}$$

where $\|V\| = \left(\iint_s |V|^2 \, dS\right)^{1/2}$ is the norm of V, $\overline{\boldsymbol{V}}$ is the climatological mean at 850 hPa, and $\overline{\boldsymbol{V}}_{1,7}$ represents the climatological mean for January and July, respectively. A $DNS \geq 2$ identifies monsoonal regions with wind reversals exceeding 90° between winter and summer.

3. Results

3.1. Seasonal Cycle of Landfall in the ENP

We first examine the climatological seasonal cycle of monthly genesis and landfall count. Figures 1a and 1b show all storm tracks (solid lines for landfall events) for HLY (LLY), and Figure 1c shows the time series of N_{lf} with HLY and LLY marked. The HLY years have 196 storms, with 49 being major hurricanes ($v_{\max} \geq 50.0$ m/s), and the LLY has 238 storms, with 59 major hurricanes.

In our framework, there are two drivers of variations in landfall: (a) variations in genesis, that is, more landfalls due to more storms; and (b) variations in landfall probability, that is, an increased likelihood for a given genesis event to make landfall due to both changes in the steering winds and in genesis location. To test the first, Figure 1d shows the monthly mean genesis. Annual mean genesis is quite similar in LLY and HLY composites as compared to the climatological mean, with HLY having a slightly higher number of storms ($\overline{N_{gen,\,\text{HLY}}} = 16.33$ vs. $\overline{N_{gen,\,\text{LLY}}} = 14.88$). The HLY are close to the climatology except in the early season, with slightly higher genesis in May and June but fewer genesis in July. Overall, though, these differences are small.

There is a marked contrast in the seasonal cycle of landfall counts as compared to genesis. First, the ENP exhibits a bimodal distribution of landfalls (Figure 1e) but not of genesis (Figure 1d), with one peak in the early season (June) and another in the late season (September and October), along with a significant drop in July and August. Second, the HLY and LLY composites differ strongly: in the HLY composite, this bimodal distribution is enhanced, whereas in the LLY composite this structure is lost entirely, including zero landfalls during the first climatological peak in June. The 4 months that contribute the most to the differences between HLY and LLY are June, August, September, and October.

Taken together, then, variations in landfall count appear to be driven not by variations in overall genesis count but by variations in landfall probability (Equation 1), which we probe further next.

3.2. Drivers of Changes in Landfall

Here, we examine the spatial distribution of HLY vs. LLY composite, focusing on the 4 months with the most differences in landfalls. Figure 2 shows the locations of all landfalls (red dots) and the regions affected by gale-force winds for all storms during HLY (LLY) in panel a (b). We observe that landfalls occur in Northwest Mexico and Central America during both groups of years, and that during HLY, storms affect regions further north in Baja California. However, only during HLY, storms make landfall in Southwest Mexico, a region that includes the three most vulnerable states based on the vulnerability index of Dominguez et al. (2021). We calculated the index using the most recent public data from the Mexican government.

To analyze this change in landfall patterns, we next use the Reynolds decomposition described in the Methods section to attribute these composite differences in landfall to changes in genesis and landfall probabilities. Figure 3a shows the contribution of each term of Equation 3 to the mean difference in landfalls between HLY and LLY years ($\Delta\overline{N_{lf}}$, i.e. difference between the red and blue curve in Figure 1d) for the 4 months that the two

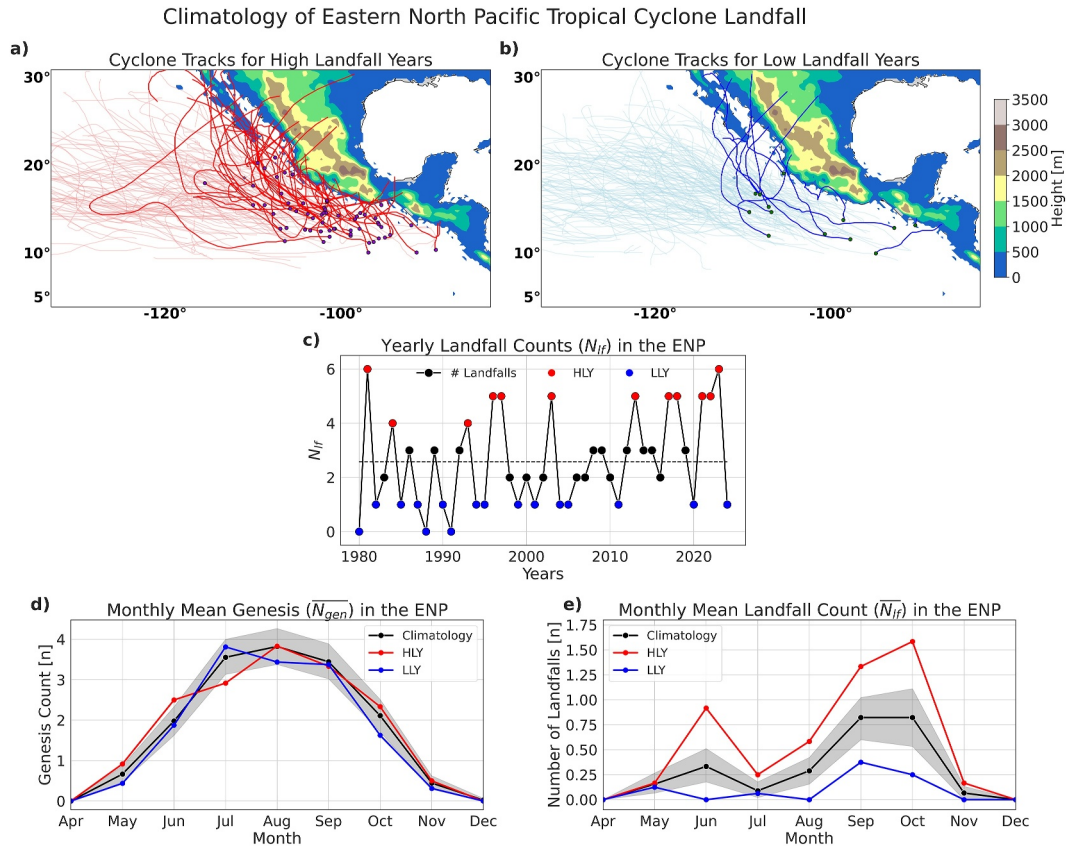

Figure 1. Climatology of Eastern North Pacific Tropical Cyclones. Panel (a, b) show all the tracks of TCs during high (low) landfall years. Semi-transparency highlights the tracks that make landfall; for landfall tracks, their genesis point is also plotted. In panel (c), the solid line is a time series of the annual number of landfalls, while the dashed line represents the mean. (d, e) show the monthly mean genesis and number of landfalls, respectively, for the climatology (black with 95% confidence interval), high (red), and low (blue) landfall years.

composites differ the most. The results indicate that variations in landfall probability account for most of the difference in landfall counts.

To examine the contribution of steering winds to the high number of landfalls during HLY years, hereafter we utilize a slightly different composite of years based on high and low landfall probabilities (HP_{lf}Y and LP_{lf}Y). This approach allows us to better capture the signal of the environmental flow that directs TCs toward land. Figure S1 in Supporting Information S1 shows the time series of p_{lf}, each group consisting of 11 years. Most of the HP_{lf}Y and LP_{lf}Y are part of the HLY and LLY, respectively, but limiting the data set to the most extreme p_{lf} years reduces the smoothing effect inherent in averaging over a larger data set, thereby enhancing the signal associated with steering winds. Note that the results are qualitatively consistent with those from the HLY/LLY composites (see Figure S2 in Supporting Information S1).

Figure 3b shows the spatial distribution of landfall probability differences (shaded areas) and steering wind vector differences (arrows) between the high and low landfall probability composites. The large circles indicate the mean genesis points for both groups. Landfall probability is defined for all genesis events within a given $5° \times 5°$ box (second term in Equation 3). Over the four months analyzed here, the region with the most enhanced landfalls in the p_{lf} composite is from TCs forming between 10°N to 15°N and 115°W to 95°W. This region also corresponds to the strongest wind differences in the basin, with an anomalous westerly wind for all months. October also has a southerly component to the anomalous wind; this observation aligns with findings by Corbosiero et al. (2009), who found that late-season storms have a stronger meridional steering because they are affected by mid-latitude troughs. The direction of this anomalous wind steers TCs into land, suggesting that steering winds have the highest impact on landfall probability in the basin.

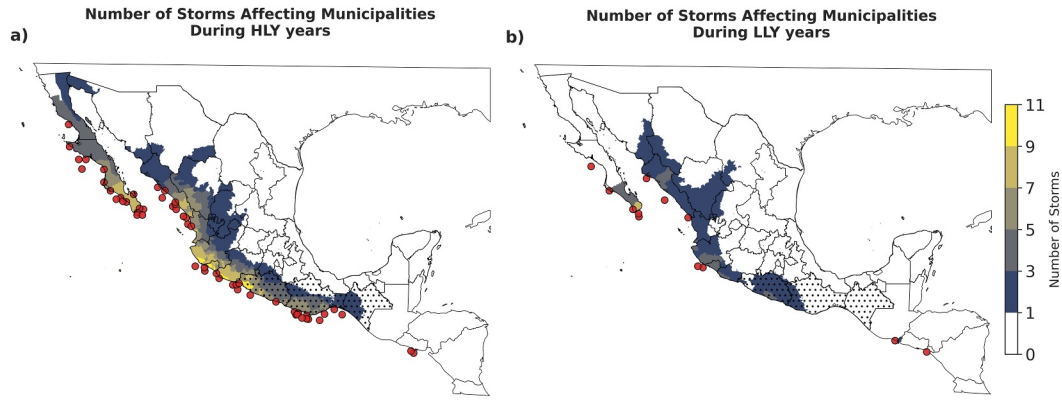

Figure 2. Regions affected by gale-force winds ($v_{max} \geq 17$ m/s) during high (left) and low (right) landfall years. The red circles show the landfall location while shadings count how many storms affected that region; the wind profile for each individual storm was calculated using the storm wind model described in the Methods section. Hashes represent the top 3 more vulnerable states in Mexico from the vulnerability index defined in Dominguez et al. (2021).

We observe that the mean genesis location is further east during all HP_{lf}Y. To quantify the impact of this shift on landfall probabilities, we calculated the change in the annual mean landfall probability (see spatial distribution in Figure S3 in Supporting Information S1) per degree of longitude and latitude, finding increases of 0.0409 per degree eastward and 0.0282 per degree northward. Multiplying these by the shifts in genesis location and dividing by Δp_{lf}, we estimate that the change in genesis location contributes 56% of the total difference in landfall probability for June, 29% for August, 32% for September, and 40% for October. These percentages indicate that while the shift in genesis location is a primary factor in June (56%), in other months, change in wind fields accounts for roughly two-thirds of the difference in p_{lf}.

Moreover, the spatial distribution from changes in genesis is generally small everywhere (Figures S4–S7 in Supporting Information S1) except for June. June, one of the peaks in the bimodal distribution, is the only month in which the TC genesis anomalies contribute a significant proportion to $\Delta\overline{N_{lf}}$ relative to the steering wind anomalies. This is because only storms that form in specific subregions (the four highlighted areas in $\overline{p_{\text{lf}}}$ in Figure S4 in Supporting Information S1) make landfall in June, and the High landfall years have a peak of extra genesis in those regions, enhancing the contribution for those extra genesis. These results suggest that while genesis location impacts landfall probability, particularly during the early season, steering flow is the most important factor and is the focus of the remainder of our analysis.

3.3. Monsoon Changes Drive Changes in Steering Flow

Finally, we aim to identify the atmospheric mechanism responsible for the change in steering flow driving changes in landfall. Figure 4a shows the climatological wind field for July, when landfalls decrease for all years in the basin (see the climatological drop in Figure 1e). We observe that, thanks to the Papagayo gap region in Nicaragua, the strong easterlies from the CLLJ (black-box region in this panel) can cross from the Caribbean Sea into the ENP, pushing TCs away from land.

Moreover, the red-stripped shadings in Figure 4a indicate the regions that exceed the critical value of the DNS index for monsoonal flows. These shadings highlight the North American Monsoon (near Baja California) and the tropical Central American Monsoon between 5° and 10°N. The tropical monsoons are related to the seasonal displacement of the ITCZ and are driven by the cross-equatorial winds; these winds from the south bend to the right after crossing the equator, becoming westerlies (Zhisheng et al., 2015).

Figure 4c shows a Hovmöller diagram for the differences in monthly mean precipitation rate between HP_{lf} and LP_{lf} years, zonally average over the green box in panel a, showing the seasonal progression of the tropical monsoon. The dipole pattern (enhanced precipitation to the north and reduced precipitation close to the equator) indicates that the ITCZ is located further north during the high landfall years, providing more space for the cross-equatorial winds to become westerlies. This shift is also observed in the red lines of 4d, which shows a time series of the 850 hPa monthly mean zonal wind speed in the red box of panel a (this region was selected because it

10.1029/2024GL113807

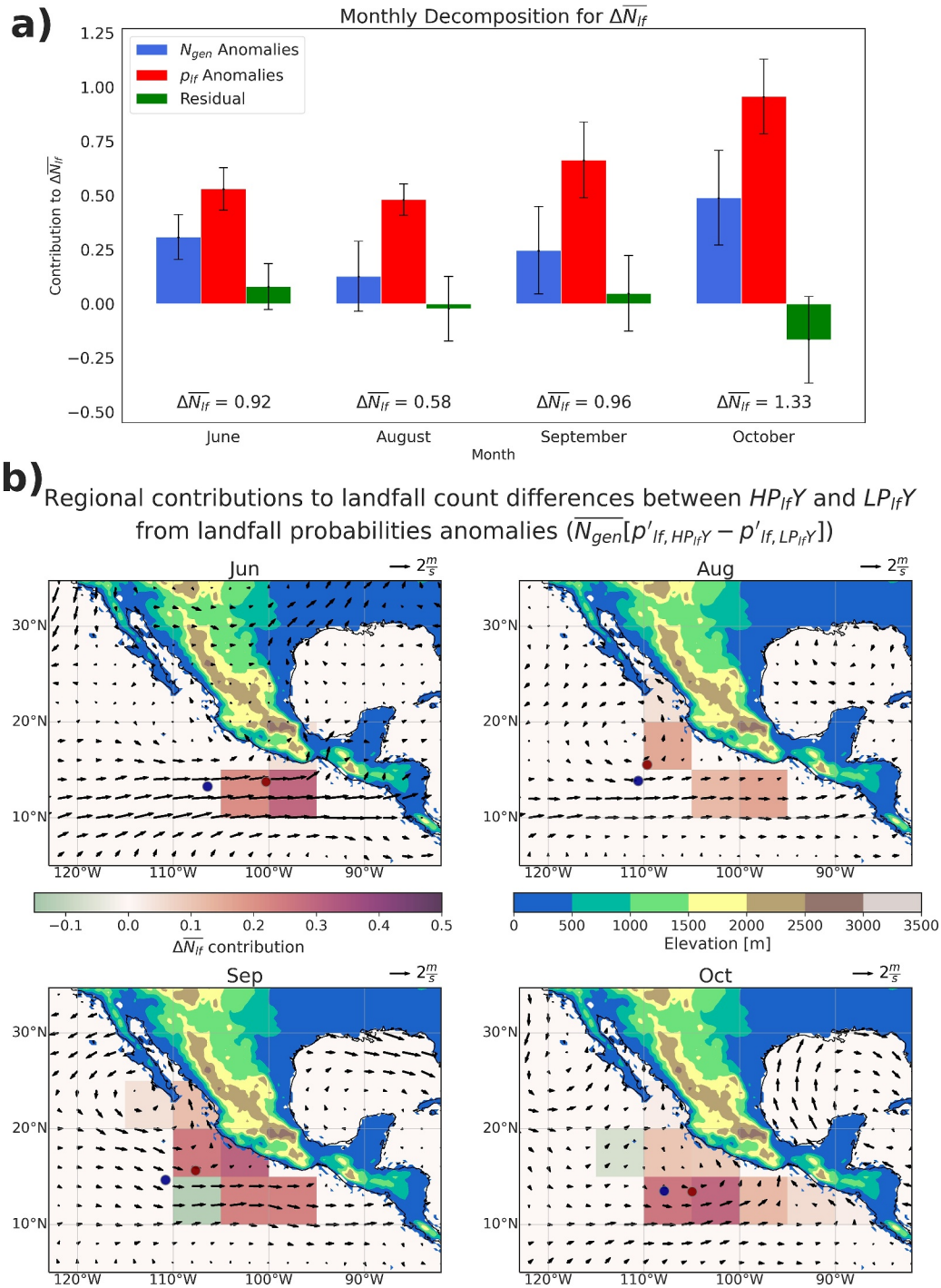

Figure 3. Panel a displays the contribution of each term in Equation 3 to the monthly mean difference in the number of landfalls during months with the greatest difference between high and low landfall years; this difference is shown at the bottom of each month. Error bars represent bootstrap-derived standard errors (n = 1,000 resamples of annual data). Panel b shows in shadings the regional contribution of landfall probabilities anomalies (red term in panel a) for 5° × 5°boxes; the wind vectors (2 m/s reference at the top of each panel) are the wind difference between the HP_{lf}Y and LP_{lf}Y. The red (blue) circles are the mean genesis location during HP_{lf}Y (LP_{lf}Y).

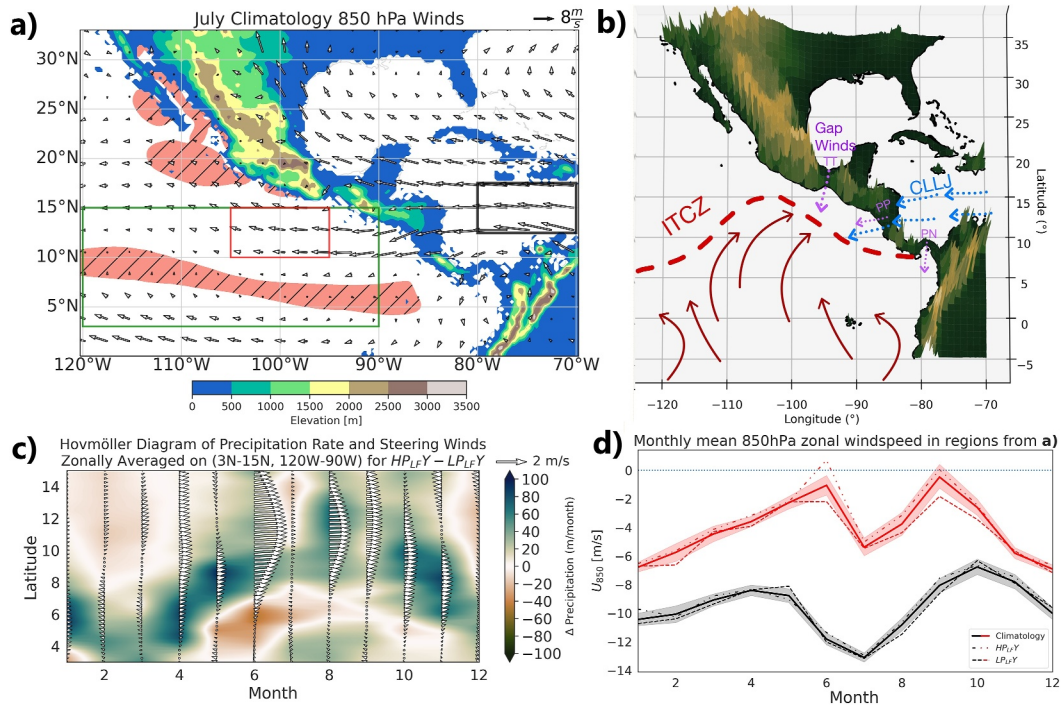

Figure 4. Panel (a) shows climatological wind vectors at 850 hPa, and elevation in shadings from ERA5. The red-striped shadings indicate regions where the DNS index exceeds significance (see Methods for details). Panel (b) is a schematic of the different factors affecting the steering winds in the basin during June, the ITCZ and its associated cross-equatorial winds in red, the CLLJ in blue, and the CAGW in purple with the gap regions marked as Tehuantepec (TT), Papagayo (PP), and Panama (PN). Panel (c) shows a Hovmöller diagram of the difference in precipitation rates and wind vectors between HP_{lf}Y and LP_{LF}Y zonally average in the green box of panel (a). Panel (d) shows a time series of the monthly mean zonal wind speed average in the boxes of the same color (black for the CLLJ region and red for the high p'_{lf} region) as in panel a; the solid line is the climatological average for the given box with 95% confidence interval, while the dashed (dashed-dotted) line shows the mean zonal velocity for the low (high) landfall probability years in the same region.

significantly affects landfalls across all months in Figure 3b). During HP_{lf}Y (dash-dotted line), the zonal winds are consistently stronger than the climatological mean (solid line with 95%CI), even shifting from easterlies to westerlies during June.

Furthermore, panel 4d reinforces the idea that topography, through the Caribbean jet, is responsible for the bimodal distribution of landfalls. As the season progresses, the ITCZ moves northward, weakening the trade winds with the influence of the cross-equatorial winds. However, in July, the CLLJ is at its peak intensity, centered closer to Central America and at a higher altitude (850 hPA compared to 925 hPa during Winter) (Wang, 2007), consistently affecting the steering winds in the ENP and counteracting the effects of the monsoon. Additionally, while the CLLJ does exhibit interannual variability, the differences between HP_{lf} and LP_{lf} years are not statistically significant from June through October, indicating that the variations in the red box are mainly due to changes in the monsoonal winds.

4. Discussion

Here, we showed that the ENP has a bimodal distribution of landfalls due to the effects of enhanced easterly winds in July from the influence of the CLLJ. Previous work by Fu et al. (2021) demonstrated the importance of topography in regulating TC activity in the region. Specifically, their simulations indicated an anomalous westerly flow in the absence of the mountain gap (see their Figure S4m), which suggests the gap's role in allowing strong easterly winds to cross into the ENP. However, it is important to note that these simulations did not accurately replicate the tropical monsoon compared to ERA5 (not shown, data provided by Dan Fu). Our analysis with reanalysis data suggests that the mountain gaps allow the strong winds from the CLLJ, through the Papagayo

gap in Nicaragua, to significantly affect the steering winds in the ENP, thereby making it more difficult for storms to make landfall in July.

We decomposed landfall counts into contributions from genesis and landfall probability and showed that the difference in the number of landfalls between high and low landfall years is driven primarily by anomalies in landfall probabilities. These anomalies are predominantly located in regions that correspond with the strongest wind differences in June, August, September, and October, suggesting that steering winds are the main driver in landfall probability in the ENP. Our analysis suggests that a more northern than usual ITCZ results in these enhanced steering winds, which allows cross-equatorial winds to become westerly and steer storms toward the vulnerable region of Southwest Mexico.

The potential for large-scale climate drivers to predict landfall variability is important but beyond the scope of this manuscript; however, we provide preliminary insights here. Previous studies suggest ENSO (La Niña) would have a strong correlation with landfall probability by favoring near-land genesis (Fu et al., 2017) and shifting the ITCZ northward (Magaña et al., 2003). To briefly explore this topic, we performed correlation analyses with various ENSO indices but found no significant relationship with p_{lf}. Figure S8 in Supporting Information S1 shows that although La Niña produces strong westerlies during August-September, these conditions are absent in June and October, key for HLY, suggesting that ENSO is not the main driver of the observed steering winds. We performed a Wilcoxon rank test between the SST and wind fields for the HP_{lf}Y and LP_{lf}Y (Figure S9 in Supporting Information S1). The results show no statistically significant SST differences in the ENSO region, although some warming anomalies appear in the northern and southern Pacific (resembling the IPO) and the Atlantic Niño region. Moreover, the anomalous westerlies discussed in this work are significant for June, which could indicate an earlier onset of the monsoon circulation rather than a stronger monsoon. Finally, we identified a statistically significant upward trend in landfall counts, with an increase of 0.406 landfalls per decade (p - value $= 0.039$), which may reflect the IPO's role in modulating ENP TC activity as previously noted by Zhao et al. (2020). Future research should further investigate the role of these large-scale climate drivers in modulating the steering wind patterns identified in this study.

Conflict of Interest

The authors declare no conflicts of interest relevant to this study.

Data Availability Statement

The tropical cyclones IBTrACS data was downloaded from Gahtan et al. (2024). The surface, pressure level, and mean fluxes monthly mean ERA5 reanalysis data from 1980 to 2024 were read online from NCAR database through the THREDDS Data Server (ECMWF, 2019). The main storm wind model was downloaded from Github at https://github.com/geanders/stormwindmodel. The two indices needed for the calculation of the vulnerability index ("Índice de Rezago Social" from CONEVAL and "Índice de Marginación" from CONAPO) are part of the open data from the Mexican Government and can be downloaded from https://datos.gob.mx/busca/dataset. Processed data and code to make the figures of this manuscript are publicly available at Ocegueda Sanchez et al. (2025).

Acknowledgments
This work is supported, in part, by the U.S. National Science Foundation NSF AGS Grant 1945113, and J.A. Ocegueda Sanchez is also supported by the Purdue-CONAHCYT Fellowship Program.

References

Anderson, G. B., Schumacher, A., Guikema, S., Quiring, S., Ferreri, J., & Tennant, E. (2021). stormwindmodel: Model tropical cyclone wind speeds. (Rpackageversion0.1.5.9. Parametric model for tropical cyclone wind field modeling). Retrieved from https://github.com/geanders/stormwindmodel

Boucharel, J., Jin, F.-F., Lin, I., Huang, H.-C., & England, M. H. (2016). Different controls of tropical cyclone activity in the eastern Pacific for two types of El Niño. *Geophysical Research Letters*, *43*(4), 1679–1686. https://doi.org/10.1002/2016gl067728

Camargo, S. J., Robertson, A. W., Barnston, A. G., & Ghil, M. (2008). Clustering of Eastern North Pacific tropical cyclone tracks: ENSO and MJO effects. *Geochemistry, Geophysics, Geosystems*, *9*(6). https://doi.org/10.1029/2007gc001861

Camargo, S. J., Robertson, A. W., Gaffney, S. J., Smyth, P., & Ghil, M. (2007). Cluster analysis of typhoon tracks. Part II: Large-scale circulation and ENSO. *Journal of Climate*, *20*(14), 3654–3676. https://doi.org/10.1175/jcli4203.1

Carr, L. E., & Elsberry, R. L. (1995). Monsoonal interactions leading to sudden tropical cyclone track changes. *Monthly Weather Review*, *123*(2), 265–290. https://doi.org/10.1175/1520-0493(1995)123<0265:miltst>2.0.co;2

Chan, J. C. (2005). The physics of tropical cyclone motion. *Annual Review of Fluid Mechanics*, *37*(1), 99–128. https://doi.org/10.1146/annurev.fluid.37.061903.175702

Chavas, D. R., Lin, N., Dong, W., & Lin, Y. (2016). Observed tropical cyclone size revisited. *Journal of Climate*, *29*(8), 2923–2939. https://doi.org/10.1175/jcli-d-15-0731.1

Chavas, D. R., Lin, N., & Emanuel, K. (2015). A model for the complete radial structure of the tropical cyclone wind field. Part I: Comparison with observed structure. *Journal of the Atmospheric Sciences*, *72*(9), 3647–3662. https://doi.org/10.1175/jas-d-15-0014.1

Collins, J. M., & Mason, I. (2000). Local environmental conditions related to seasonal tropical cyclone activity in the northeast Pacific basin. *Geophysical Research Letters*, *27*(23), 3881–3884. https://doi.org/10.1029/2000gl011614

Collins, J. M., & Mason, I. M. (2003). Seasonal environmental conditions related to hurricane activity in the northeast Pacific basin. *The New England-St. Lawrence Valley Geographical Society*, *33*, 44–50.

Corbosiero, K. L., Dickinson, M. J., & Bosart, L. F. (2009). The contribution of eastern north Pacific tropical cyclones to the rainfall climatology of the southwest United States. *Monthly Weather Review*, *137*(8), 2415–2435. https://doi.org/10.1175/2009mwr2768.1

DeMaria, M., Franklin, J. L., Zelinsky, R., Zelinsky, D. A., Onderlinde, M. J., Knaff, J. A., et al. (2022). The national hurricane center tropical cyclone model guidance suite. *Weather and Forecasting*, *37*(11), 2141–2159. https://doi.org/10.1175/waf-d-22-0039.1

Dominguez, C., Jaramillo, A., & Cuéllar, P. (2021). Are the socioeconomic impacts associated with tropical cyclones in Mexico exacerbated by local vulnerability and ENSO conditions? *International Journal of Climatology*, *41*(S1), E3307–E3324. https://doi.org/10.1002/joc.6927

Dominguez, C., & Magaña, V. (2018). The role of tropical cyclones in precipitation over the tropical and subtropical North America. *Frontiers in Earth Science*, *6*, 312622. https://doi.org/10.3389/feart.2018.00019

Emanuel, K., Ravela, S., Vivant, E., & Risi, C. (2006). A statistical deterministic approach to hurricane risk assessment. *Bulletin of the American Meteorological Society*, *87*(3), 299–314. https://doi.org/10.1175/bams-87-3-299

European Centre for Medium-Range Weather Forecasts (ECMWF). (2019). ERA5 reanalysis (monthly mean 0.25 degree latitude-longitude grid) (updated yearly) [Dataset]. *Research Data Archive at the National Center for Atmospheric Research, Computational and Information Systems Laboratory*. https://doi.org/10.5065/P8GT-0R61

Fu, D., Chang, P., & Patricola, C. M. (2017). Intrabasin variability of east Pacific tropical cyclones during ENSO regulated by Central American gap winds. *Scientific Reports*, *7*(1), 1658. https://doi.org/10.1038/s41598-017-01962-3

Fu, D., Chang, P., Patricola, C. M., Saravanan, R., Liu, X., & Beck, H. E. (2021). Central American mountains inhibit eastern North Pacific seasonal tropical cyclone activity. *Nature Communications*, *12*(1), 4422. https://doi.org/10.1038/s41467-021-24657-w

Gahtan, J., Knapp, K. R., Schreck, C. J. I., Diamond, H. J., Kossin, J. P., & Kruk, M. C. (2024). International best track archive for climate stewardship (IBTrACS) project, version 4.01. EP subset [Dataset]. *NOAA National Centers for Environmental Information*. (Downloaded CSV format on: 2025-02-20). https://doi.org/10.25921/82ty-9e16

Geen, R., Bordoni, S., Battisti, D. S., & Hui, K. (2020). Monsoons, ITCZS, and the concept of the global monsoon. *Reviews of Geophysics*, *58*(4), e2020RG000700. https://doi.org/10.1029/2020rg000700

Huaman, L., Schumacher, C., & Sobel, A. H. (2022). Assessing the vertical velocity of the East Pacific ITCZ. *Geophysical Research Letters*, *49*(1), e2021GL096192. https://doi.org/10.1029/2021gl096192

Ito, K., Wu, C.-C., Chan, K. T., Toumi, R., & Davis, C. (2020). Recent progress in the fundamental understanding of tropical cyclone motion. *Journal of the Meteorological Society of Japan. Ser. II*, *98*(1), 5–17. https://doi.org/10.2151/jmsj.2020-001

Juarez-Torres, M., & Puigvert, J. (2021). *The effect of tropical cyclones on economic activities: Micro level evidence from Mexico for secondary and tertiary activities (Tech. Rep. No. 2021-24). Working Papers*. Banco de México.

Kim, H.-M., Webster, P. J., & Curry, J. A. (2011). Modulation of North Pacific tropical cyclone activity by three phases of ENSO. *Journal of Climate*, *24*(6), 1839–1849. https://doi.org/10.1175/2010jcli3939.1

Li, J., & Zeng, Q. (2003). A new monsoon index and the geographical distribution of the global monsoons. *Advances in Atmospheric Sciences*, *20*(2), 299–302. https://doi.org/10.1007/s00376-003-0016-5

Li, W., Li, L., & Deng, Y. (2015). Impact of the Interdecadal Pacific Oscillation on tropical cyclone activity in the North Atlantic and Eastern North Pacific. *Scientific Reports*, *5*(1), 12358. https://doi.org/10.1038/srep12358

Magaña, V. O., Vázquez, J. L., Pérez, J. L., & Pérez, J. B. (2003). Impact of El Niño on precipitation in Mexico. *Geofísica Internacional*, *42*(3), 313–330.

Ocegueda Sanchez, J. A., Chavas, D. R., & Jones, J. (2025). Data for interannual variability of tropical cyclone landfalls in the eastern North Pacific [Dataset]. https://doi.org/10.4231/DGRQ-MC61

Romero-Vadillo, E., Zaytsev, O., & Morales-Pérez, R. (2007). Tropical cyclone statistics in the northeastern Pacific. *Atmósfera*, *20*(2), 197–213.

Sobel, A. H., Wing, A. A., Camargo, S. J., Patricola, C. M., Vecchi, G. A., Lee, C.-Y., & Tippett, M. K. (2021). Tropical cyclone frequency. *Earth's Future*, *9*(12), e2021EF002275. https://doi.org/10.1029/2021ef002275

Wang, C. (2007). Variability of the Caribbean low-level jet and its relations to climate. *Climate Dynamics*, *29*(4), 411–422. https://doi.org/10.1007/s00382-007-0243-z

Willoughby, H. E., Darling, R., & Rahn, M. (2006). Parametric representation of the primary hurricane vortex. Part II: A new family of sectionally continuous profiles. *Monthly Weather Review*, *134*(4), 1102–1120. https://doi.org/10.1175/mwr3106.1

Xie, S.-P., Xu, H., Kessler, W. S., & Nonaka, M. (2005). Air–sea interaction over the eastern Pacific warm pool: Gap winds, thermocline dome, and atmospheric convection. *Journal of Climate*, *18*(1), 5–20. https://doi.org/10.1175/jcli-3249.1

Yang, J.-C., Lin, X., & Xie, S.-P. (2017). A transbasin mode of interannual variability of the central American gap winds: Seasonality and large-scale forcing. *Journal of Climate*, *30*(20), 8223–8235. https://doi.org/10.1175/jcli-d-17-0021.1

Zhao, J., Zhan, R., Wang, Y., Xie, S.-P., & Wu, Q. (2020). Untangling impacts of global warming and Interdecadal Pacific Oscillation on long-term variability of North Pacific tropical cyclone track density. *Science Advances*, *6*(41), eaba6813. https://doi.org/10.1126/sciadv.aba6813

Zhisheng, A., Guoxiong, W., Jianping, L., Youbin, S., Yimin, L., Weijian, Z., et al. (2015). Global monsoon dynamics and climate change. *Annual Review of Earth and Planetary Sciences*, *43*(1), 29–77. https://doi.org/10.1146/annurev-earth-060313-054623

References From the Supporting Information

Williams, I. N., & Patricola, C. M. (2018). Diversity of ENSO events unified by convective threshold sea surface temperature: A nonlinear ENSO index. *Geophysical Research Letters*, *45*(17), 9236–9244. https://doi.org/10.1029/2018gl079203